Catalysis Today 158 (2010) 156–161

Contents lists available at ScienceDirect

Catalysis Today

journal homepage: www.elsevier.com/locate/cattod

Structural flexibility in ~$SbVO_4$

Angel R. Landa-Cánovas [a,*], F. Javier García-García [b], Staffan Hansen [c]

[a] Instituto de Ciencia de Materiales de Madrid, CSIC, E-28049 Madrid, Spain
[b] Lehrstuhl für Festkörperchemie, Institut für Physik, Universität Augsburg, Universitätsstrasse 1, D-86159 Augsburg, Germany
[c] Division of Polymer and Materials Chemistry, Department of Chemistry, Lund University, Chemical Center, P.O. Box 124, SE-221 00 Lund, Sweden

ARTICLE INFO

Article history:
Available online 2 June 2010

Keywords:
Catalyst
Propane ammoxidation
$SbVO_4/Sb_2O_4$ system
Non-stoichiometry
Structural flexibility

ABSTRACT

~$SbVO_4$ is a well known catalyst used for the ammoxidation of propane to acrylonitrile. However, little importance is usually given to the structural flexibility exhibited by the ~$SbVO_4$ phase, which has rutile-type structure and can accommodate up to 1/8 of cation vacancies. In this work we highlight the great structural flexibility exhibited by this phase accommodating the changes in the oxidation state of vanadium which is accompanied by the introduction of cation vacancies. Besides, it presents a wide range of compositional non-stoichiometry, ranging from a 1/1 vanadium/antimony molar ratio to almost 1/0. It is carried out in a soft way and does not involve the creation of extended structural defects but more subtle structural changes such as long-range order, structural modulations and short-range order.

1. Introduction

Acrylonitrile is an important intermediate for the preparation of fibres, rubbers and other valuable products. At present, acrylonitrile is produced by the catalytic ammoxidation of propylene [1–3]. Recently, much effort has been invested in new catalysts that could enable the efficient direct synthesis of acrylonitrile from propane since it would decrease the acrylonitrile price by 20% [4].

A high selectivity in these processes has been exhibited by vanadium–antimony mixed oxides as catalysts for propane ammoxidation. Vanadium site isolation as well as cooperation with Sb_2O_4 is considered to be important for the catalysis [5–17]. These catalysts typically contain several phases such as rutile-type ~$SbVO_4$, Sb_2O_4 and V_2O_5, depending on the preparation method used and on the Sb/V ratio. Rutile-type ~$SbVO_4$ has been demonstrated to be cation deficient [18,19].

The rutile structure is one of the first crystal structures described as Vegard determined in 1916 the structures of TiO_2 and SnO_2 [20]. A great variety of compounds exhibit this structure and many derivatives are known consisting either of cation ordering, anion ordering or on distortions of the coordination polyhedra [21]. Non-stoichiometric compounds are well known when anion deficiency is introduced. In these, the rutile structure accommodates the non-stoichiometry by means of Crystallographic Shear Planes (CSPs) where locally the rutile structure collapses into corundum-type structure, i.e., edge-sharing octahedra change to face-sharing ones [22].

The purpose of this work is to show the remarkable structural flexibility exhibited by ~$SbVO_4$ phase under different conditions, accommodating different vanadium oxidation states and up to 1/8 cation vacancies in a soft way through structural modulation and without the creation of defects nor any collapse of the structure.

2. Materials and methods

The samples were prepared at 800 °C in a quartz tube furnace under a flow of different mixtures of nitrogen and oxygen ranging from pure nitrogen to pure oxygen. The samples were primarily characterised by powder X-ray diffraction methods.

SEM studies were carried out using a JEM 6400 microscope operating at 20 kV. TEM specimens were prepared from sonical dispersions of the corresponding samples in butanol. One drop of each suspension was deposited on a copper grid covered with a holey carbon film.

Conventional TEM experiments were carried out on a JEOL 2000FX TEM microscope running at 200 kV and equipped with a LINK AN10000 analyser system. HRTEM studies were carried out in a JEM 4000EX microscope working at 400 kV and with 1.8 Å point resolution.

3. Results and discussion

Rutile-type ~$SbVO_4$, although apparently exhibiting a very simple structure, in reality presents an unexpected complexity imposed by the oxidation states of the cations. Magnetic susceptibility measurements [23] excluded the presence of V^{5+} and of Sb^{3+}. Mössbauer spectroscopy confirmed the presence of Sb^{5+} [24] while ESR indicated the existence of V^{3+} or V^{4+} depending on the reaction

* Corresponding author.
E-mail address: landa@icmm.csic.es (A.R. Landa-Cánovas).

0920-5861/$ – see front matter © 2010 Elsevier B.V. All rights reserved.
doi:10.1016/j.cattod.2010.04.027

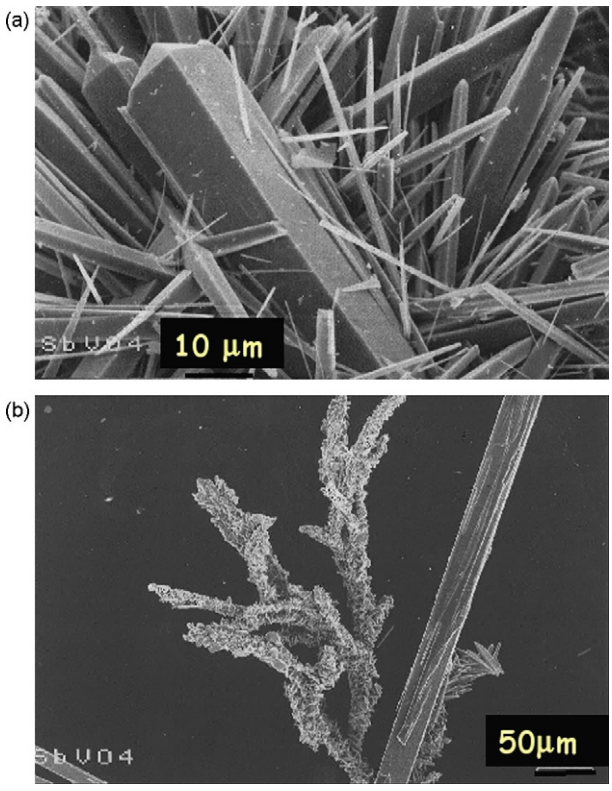

Fig. 1. (a) SEM micrograph of typically shaped $SbVO_4$ rutile-type crystals and (b) crystallite agglomeration of oxidized ~$SbVO_4$.

conditions [25]. Bond-valence summations [18] and X-ray energy-dispersive spectroscopy (XEDS) [19] revealed that only Sb^{5+}, V^{4+} and V^{3+} were present. The presence of cation vacancies is possible through the existence of V^{4+}.

The first sample series prepared in Ref. [19] aimed directly to investigate the generation of cation vacancies in the ~$SbVO_4$ phases:

$$V_2O_5 + Sb_2O_3\,(1:1) \rightarrow \sim SbVO_4 + (Sb_2O_4)$$

This series was prepared at 800 °C under a flow of gas at different oxygen pressures, ranging from pure oxygen-free nitrogen flow to pure oxygen at 1 atmosphere of pressure. Powder X-ray diffraction patterns only showed typical rutile-type maxima apart from the diffraction peaks from the excess of Sb_2O_4. Although in general the rutile crystals obtained maintained the well known prismatic shape typical of rutile, see the SEM micrograph of Fig. 1a, when the samples were prepared under high oxygen partial pressures their morphology changed drastically to arborescent or tree-like agglomeration of crystallites, see Fig. 1b. This could already suggest that subtle changes are introduced in the rutile-type structure due to the preparation conditions.

The transmission electron microscopy study of these sample reveals the complexity of the crystal chemistry of these phases. Apart from the Sb_2O_4 crystals, which consist of disordered intergrowths of the α-Sb_2O_4, and β-Sb_2O_4 as already described in [26], see Fig. 2, the rutile-type crystals revealed a complex behaviour. Different rutile-type ~$SbVO_4$ samples prepared under different atmospheres were studied by selected area electron diffraction (SAED) which consists of using an aperture below the objective lens to select an area of the crystal to diffract and producing very sharp diffraction spots. At very low oxygen pressures weak superlattice reflections appeared doubling the rutile-type lattice, see Fig. 3a. When very little oxygen was allowed during the synthesis process these superlattice reflections smeared out giving rise to weak and

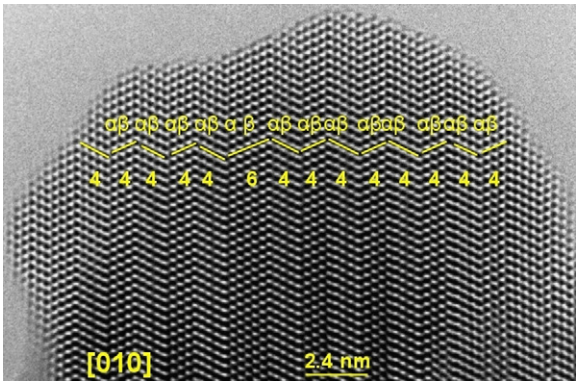

Fig. 2. HRTEM micrograph of a crystal of Sb_2O_4 showing a disordered intergrowth of the α and β forms.

diffuse intensity lines running parallel to the b axis, see Fig. 3b. Any diffraction satellites or diffuse streaks disappear as the oxygen pressure is increased up to the normal air pressure, Fig. 3c. Then, weak satellite reflections appear which are at almost $1/4(1\,1\,1)^*$ but still incommensurable due to a modulation of the rutile-type structure, as shown in Fig. 3d. The intensity of these reflections increases as the oxygen pressure is increased up to pure oxygen flow during the synthesis procedure.

By changing the oxygen pressure during the synthesis we are playing with the vanadium oxidation state and introducing cation vacancies according to the following reaction mechanism:

$$4V^{3+} \rightarrow 3V^{4+} + \square$$

where □ indicates a cation vacancy. Therefore, all the subtle diffraction phenomena that we are observing are related with the accommodation of the non-stoichiometry, i.e., of the cation vacancies and the different vanadium atoms with different oxidation states, in the rutile-type structure. The intense effect observed in the electron diffraction patterns induce us to attribute the main cause to the cation vacancies accommodation since electron diffraction would not be so sensitive to only the change in oxidation state of the vanadium atoms.

The reduced phase was determined to be $Sb_{0.9}V_{1.1}O_4$ by means of XEDS experiments [19] and its atomic structure has been solved by Landa-Canovas et al. [27] using powder X-ray diffraction, electron diffraction and HRTEM methods. The rutile superstructure was indexed on the unit cell $a = \sqrt{2}a_r$, $b = \sqrt{2}b_r$, $c = 2c_r$, where subindex r refers to the original rutile unit cell. The space group $I4_1md$ was determined by means of convergent beam electron diffraction and finally an atomic model fulfilling all the observed data was proposed where antimony and vanadium atoms alternate along the *c* axis, see Fig. 4. The superstructure can also be described as two interpenetrated spirals of vanadium and antimony cations running clockwise or anticlockwise along *c*. Notice that the cation arrangement is the same as observed in zircon but the anion sublattice changes, the cations being either inside oxygen-cornered bisdisphenoids (eight-cornered polyhedra) or inside tetrahedra instead of in the centre of oxygen-cornered octahedra [22].

This sample proved to be very unstable under the electron beam as antimony oxide was leaving the crystals under the observation in the microscope. From these results it was deduced that most of vanadium was in oxidation state III, while antimony kept the oxidation state V and no vacancies were observed. The density of this phase, measured with helium in a gas pycnometer indicated the absence of cation vacancies [19].

When a little amount of oxygen was allowed during the synthesis the observed cation ordering was rapidly destroyed leading first from superlattice spots to diffuse intensity streaks observed only

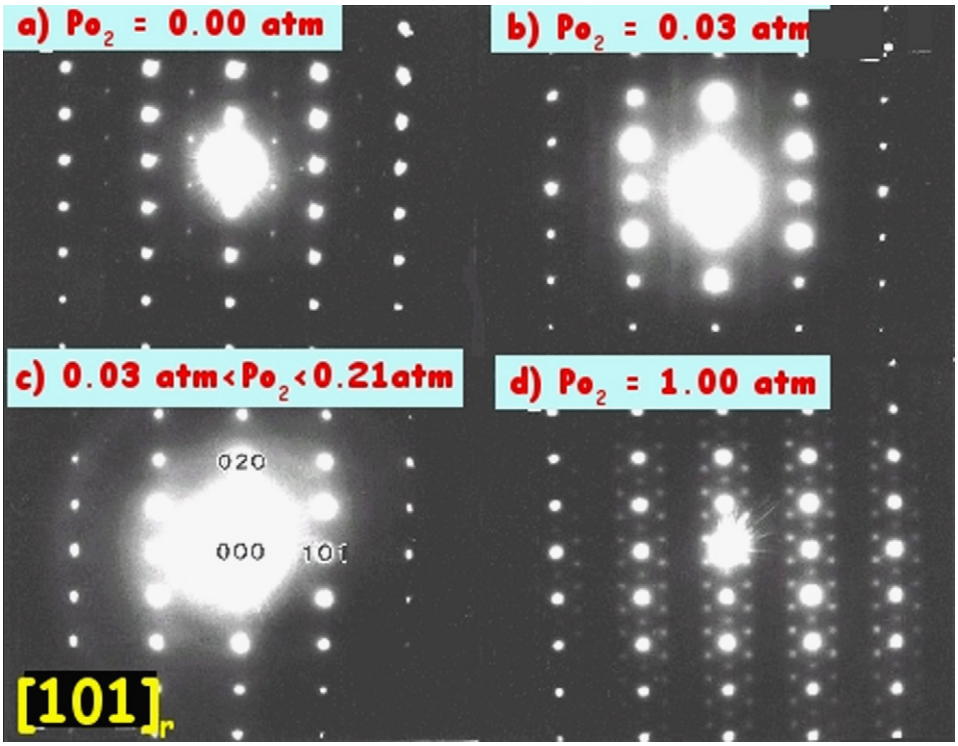

Fig. 3. SAED patterns of ~$SbVO_4$ crystals oriented along the [1 0 1] basic rutile direction and prepared at different oxygen pressures indicated in the upper-left part of every diagram.

by electron diffraction, see Fig. 3b. The reason for this rapid degradation of the cationic ordering can be found in the bond-valence sums carried out by Hansen et al. [18] which revealed that when we introduce a vacancy in the ~$SbVO_4$ rutile structure, then the oxygen atoms surrounding it will be underbonded and since they are coordinated to other two cations, in order to compensate this underbonding, they will prefer to be coordinated to two antimony atoms better than to two vanadium atoms. This rearrangement will rapidly destroy the alternation of Sb and V observed in reduced $Sb_{0.9}V_{1.1}O_4$. The fact that we observe diffuse streaks as the first steps of the order degeneration is due to the presence short-range order, i.e., to the permanence of small clusters or islands diluted inside the basic rutile framework keeping the previous cationic order.

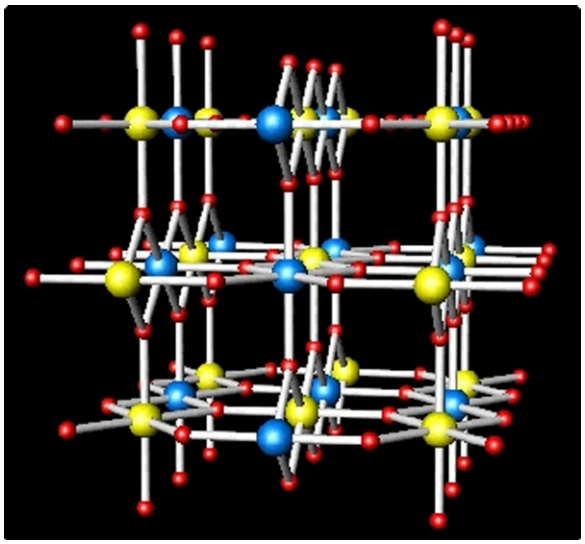

Fig. 4. Schematic drawing of the atomic structure of reduced $Sb_{0.9}V_{1.1}O_4$. Blue and yellow spheres indicate V and Sb atoms. In red are depicted the oxygen atoms. (For interpretation of the references to colour in this figure legend, the reader is referred to the web version of the article.)

At high partial oxygen pressures, i.e., from the samples prepared in air to the pure oxygen flow ones there appear weak satellite reflections due to an incommensurate modulation of the structure, complicating very much the SAED patterns, see Fig. 5. This modulation is very close to a commensurate one and the reciprocal lattice can be described as $\mathbf{G} \pm m\mathbf{q}$, $\mathbf{G}$ being the basic rutile reflections, m an integer number and $\mathbf{q}$ the modulation vector given by:

$$\mathbf{q} \approx \pm\left(\frac{1}{4}\right)a^* \pm \left(\frac{1}{4}\right)b^* \pm \left(\frac{1}{4}\right)c^*$$

As a commensurate approximation the modulation would lead to a rutile supercell $a = 2\sqrt{2}a_r$, $b = 2\sqrt{2}\ b_r$, $c = 4\ c_r$, the subindex r referring to the basic rutile unit cell. Solving this modulated structure is quite complicated and requires crystallography in at least four dimensions but all the evidence we have suggests that the structural modulation is mainly produced by the arrangement of the cation vacancies on top of a rutile basic structure [28]. This is observed in the HRTEM image shown in Fig. 6, where the white spots can be assigned to the cationic positions in basic rutile structure and the superimposed dark bands can be attributed to sinusoidal population waves of vacancies in a similar way as it is described for La_3S_4, etc. [29] The modulation contrast runs in a "soft way" on top of the basic rutile structure and it is not locked to it, i.e., the dark bands are not always located on the same position relative to the basic lattice. Notice as well that in some places, for example at the centre of the image, small areas can be distinguished displaying what could be considered as a superstructure contrast, which does not extend longer than a few unit cells. This is due to the fact that the modulation is almost commensurate but still incommensurate and then the modulation periodicity misfits slightly with the rutile periodicity. Two intensity line scans are also presented, one along the magenta line is intended to run across the rutile cationic posi-

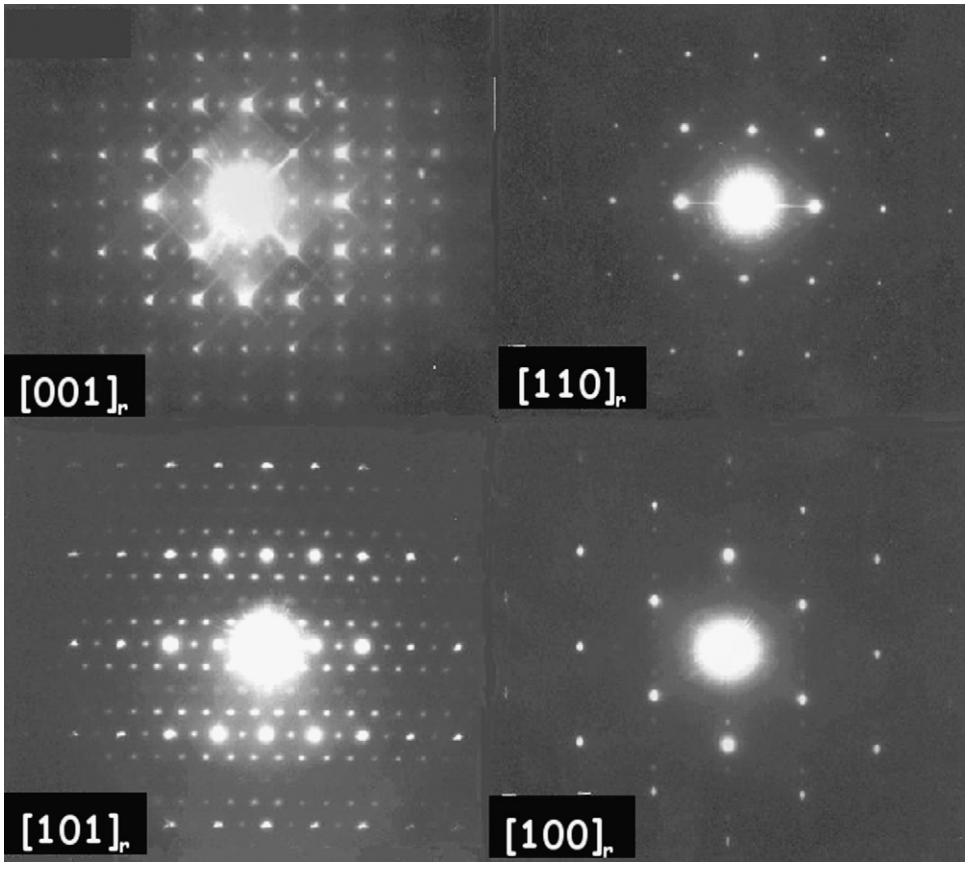

Fig. 5. SAED patterns of modulated ~$SbVO_4$ along four different crystallographic orientations indicated at the bottom left corner of each diagram.

tions and the one along the blue line mainly is to run on the vacancy modulation waves showing a wide dark sinusoidal contrast.

In these conditions most of the vanadium is oxidized to V^{4+} and we have to introduce cation vacancies in order to keep the charge balance. If all the vanadium is oxidized the phase composition has to be close to $Sb_4V_3\square O_{16}$, where □ indicates a cation vacancy. Therefore, we have introduced 1/8 of vacancies in the cation sublattice, which is, to the best of our knowledge, the highest amount

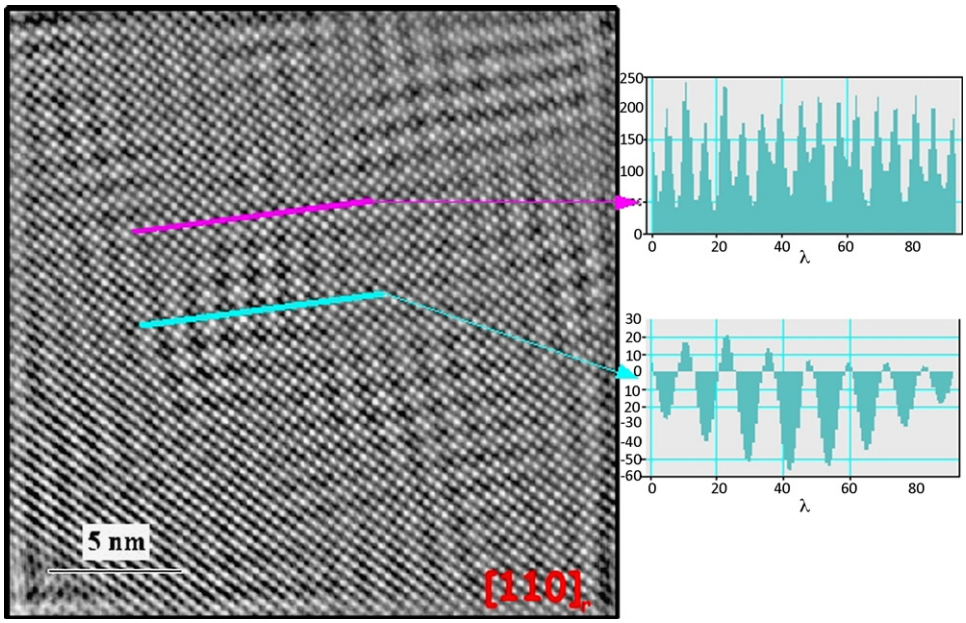

Fig. 6. HRTEM image of a crystal of oxidized ~$SbVO_4$ orientated along the [1 1 0] rutile direction. The white dots correspond to basic rutile cation positions and the superimposed dark bands to sinusoidal waves of cation vacancies. Marked in red almost commensurate areas are highlighted. The magenta and blue lines indicate the line scans whose intensity is displayed at the right of the figure. Magenta line runs across the cationic positions while the blue line runs mainly across the cation vacancy waves. (For interpretation of the references to colour in this figure legend, the reader is referred to the web version of the article.)

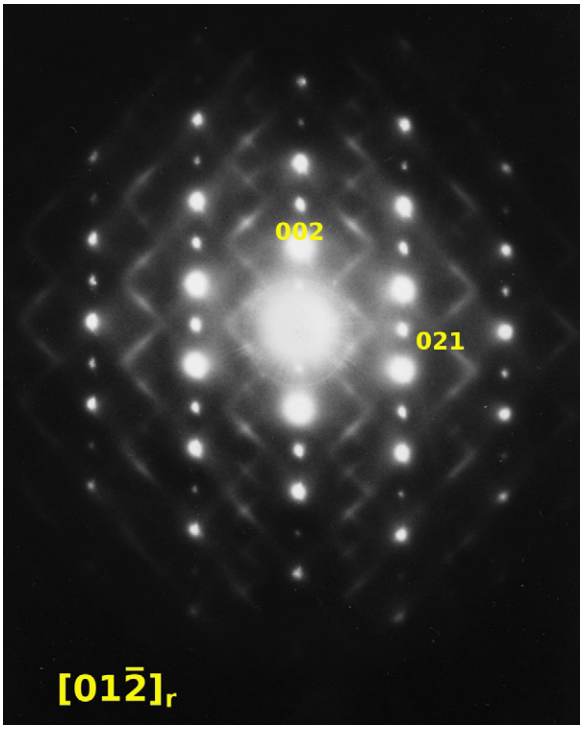

Fig. 7. SAED pattern of a crystal of $Sb_{0.2}V_{1.8}O_4$ orientated along the [0 3 1] direction displaying diffuse intensity between the basic rutile reflections.

of cation vacancies introduced in rutile and still it is accommodated in the structure in a very soft way without the introduction of any extended structural defect as it is common with certain rutiles.

The second sample series studied is:

$$V_2O_5 + Sb_2O_3\,(1:1\text{–}10:1) \rightarrow \sim SbVO_4$$

This series is synthesized at 800 °C under pure N_2 changing the nominal molar ratio between V_2O_5 and Sb_2O_3 from 1:1 to 10:1 [19]. In all the prepared samples the basic rutile structure is maintained but subtle structural changes occur along the composition range. For the 1:1 ratio the $Sb_{0.9}V_{1.1}O_4$ phase is formed with a twofold superstructure due to the order between Sb and V as mentioned previously [27]. When the amount of Sb_2O_4 decreases the superstructure satellites disappear quickly and for a significant range of composition only the rutile reflections remain visible. However, for compositions close to V_2O_4 another subtle diffraction phenomenon appears. In Fig. 7a SAED pattern from a crystal of $Sb_{0.2}V_{1.8}O_4$ shows, besides the basic rutile Bragg reflections, diffuse shapes due to the intersection of the Ewald sphere with diffuse intensity three-dimensional surfaces in the reciprocal space caused by short-range phenomena in the crystal. Apparently, antimony and vanadium atoms are not randomly distributed through the crystal but their ordering is not a long-range one as it occurred previously in $Sb_{0.2}V_{1.8}O_4$. Therefore, Sb and V order in clusters or statistically through the crystal and do not give rise to extra sharp reflections or satellites but to geometrically diffuse surfaces of diffracted intensity in the reciprocal space.

These series reveal that the existence domain of non-stoichiometric ~$SbVO_4$ is wider and complicated than previously thought as it is schematized in Fig. 8. The first series, which is the important one from the catalytic point of view was made with excess of Sb_2O_4 so it really depicts the antimony-rich limit of existence of the ~$SbVO_4$ phase as a function of the partial oxygen pressure and it is defined by the reaction mechanism:

$$4V^{3+} \rightarrow 3V^{4+} + \square \qquad (1)$$

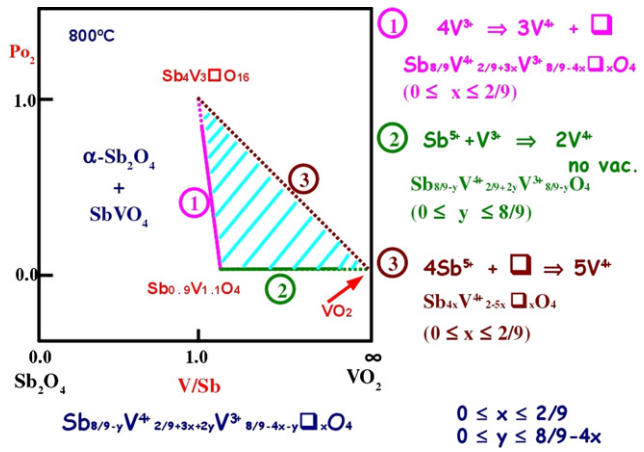

Fig. 8. Scheme showing the domain of existence of ~$SbVO_4$ as a function of composition and partial oxygen pressure at 800 °C. The three described sample series are depicted in magenta, green and dark red lines and their expressions and reaction mechanisms at the left of the scheme in the corresponding colours. The general expression for the whole domain of existence that consists on the cyan stripped region of the scheme is formulated at the bottom of the figure. (For interpretation of the references to colour in this figure legend, the reader is referred to the web version of the article.)

The composition of ~$SbVO_4$ along this line is given by the formula $Sb_{8/9}V^{4+}{}_{2/9+3x}V^{3+}{}_{8/9-4x}\square_xO_4$ ($0 \le x \le 2/9$) increasing x, or the amount of vacancies (□) and of V^{4+}, with the partial oxygen pressure. The limit is given by the total oxidation of V^{3+} to V^{4+}.

The second series explores the change of composition experienced by ~$SbVO_4$ in pure nitrogen. Along this line two V^{4+} replace an Sb^{5+} and a V^{3+} without generating or eliminating any vacancy:

$$Sb^{5+} + V^{3+} \rightarrow 2\,V^{4+} \qquad (2)$$

The general formula that describes this line is $Sb_{8/9-y}V^{4+}{}_{2/9+2y}V^{3+}{}_{8/9-y}O_4$ ($0 \le y \le 8/9$). Notice again that vacancies are not involved in this expression. One limit is practically VO_2 and the antimony-rich limit has been experimentally determined to be $Sb_{0.9}V_{1.1}O_4$.

There is a third line limiting the existence region of ~$SbVO_4$ and it is defined by the reaction mechanism:

$$4Sb^{5+} + \square \rightarrow 5\,V^{4+} \qquad (3)$$

with the general formula $Sb_{4x}V^{4+}{}_{2-5x}\square_xO_4$ ($0 \le x \le 2/9$). It is a theoretical line since we have not prepared samples along this line, but it connects the two experimental series.

Therefore, the domain of existence of ~$SbVO_4$ rutile-type phase is define by the triangle defined by these three lines as depicted in Fig. 8. The general expression that defines the composition of this phase is:

$$Sb_{8/9-y}V^{4+}{}_{2/9+3x+2y}V^{3+}{}_{8/9-4x-y}\square_xO_4 \quad (0 \le x \le 2/9,\ 0 \le y \le 8/9).$$

For samples prepared with starting compositions richer in antimony than the composition prescribed by line (1) we will have the coexistence of Sb_2O_4 and of ~$SbVO_4$. Notice that line 1 is not strictly vertical since we have observed that Sb_2O_4 is segregated as the partial oxygen pressure is lowered in the synthesis. The diagram of Fig. 8 depicts the important structural flexibility in ~$SbVO_4$ since large changes in the phase can take place, like for example introduction of up to 1/8 of cation vacancies, change of the oxidation state of vanadium atoms from 3+ to 4+ or substitution of almost all the antimony atoms by vanadium, all of them without breaking the basic rutile framework and by introducing subtle structural modifications that adapt to and accommodate the non-stoichiometry in a remarkably "soft way", i.e., without any dramatic structural change.

This structural flexibility has to be crucial for the catalytic performance of ~$SbVO_4$ since during the ammoxidation of propane to acrylonitrile important redox reactions have to occur in the surface of the rutile crystals which imply changes in the oxidation state of the vanadium atoms and these changes, even though the reaction takes place at the surface, have to be accommodated by the bulk of the crystal or at least by a surface layer on it. Besides, during many cycles the structure has to accommodate these changes without structural damage and the exhibited structural flexibility seems a good way to provide the expected performance. This would be much more difficult if the structure accommodated the non-stoichiometry through planar structural defects since they cannot be so flexible. Operando Raman Spectroscopy studies during the propane ammoxidation reaction indicate changes in the oxidation state of vanadium [30–32].

4. Conclusions

The rutile-type ~$SbVO_4$ phase exhibits a unique behaviour accepting large changes of composition, oxidation state of the vanadium atoms and the introduction of cation vacancies. This remarkable structural flexibility is accommodated in a "soft way" through structural modulations, short-range order or even periodical long-range order. It surely is related to its good performance as a catalyst in the ammoxidation of propane to acrylonitrile. The general overview given here on the complicated crystal chemistry of this system is expected to clarify some of the complicated mechanisms that are involved in the catalytic performance of ~$SbVO_4$.

Acknowledgments

Financial support through Spanish research project MAT2008-06858-C02-02 and CSIC PIE project 200860I194 is acknowledged.

References

[1] R.K. Grasselli, in: G. Ertl, H. Knözinger, J. Weitkamp (Eds.), Handbook of Heterogeneous Catalysis, Wiley-VCH, New York, 1997, p. 2302.
[2] R.K. Grasselli, Catal. Today 49 (1999) 141.
[3] R. Nilsson, T. Lindblad, A. Anderson, Catal. Lett. 29 (1994) 409.
[4] M.M. Bettarhar, G. Costentin, L. Savary, J.C. Lavalley, Appl. Catal. A 145 (1996) 1.
[5] G. Centi, R.K. Grasselli, E. Patanè, F. Trifirò, Stud. Surf. Sci. Catal. 55 (1990) 515.
[6] R.K. Grasselli, G. Centi, F. Trifirò, Appl. Catal. 57 (1990) 149.
[7] G. Centi, R.K. Grasselli, F. Trifirò, Catal. Today 13 (1992) 661.
[8] J. Nilsson, T. Lindblad, A. Andersson, C. Song, S. Hansen, Stud. Surf. Sci. Catal. 82 (1994) 293.
[9] J. Nilsson, T. Lindblad, A. Andersson, J. Catal. 148 (1994) 501.
[10] G. Centi, S. Perathoner, Appl. Catal. A 124 (1995) 317.
[11] J. Nilsson, A.R. Landa-Cánovas, S. Hansen, A. Andersson, J. Catal. 160 (1996) 244.
[12] J. Nilsson, A.R. Landa-Cánovas, S. Hansen, A. Andersson, J. Catal. 186 (1999) 442.
[13] A. Wickman, L.R. Wallenberg, A. Andersson, J. Catal. 194 (2000) 153.
[14] T. Shishido, T. Konishi, I. Matsuura, Y. Wang, K. Takaki, K. Takehira, Catal. Today 71 (2001) 77.
[15] A. Andersson, S. Hansen, A. Wickman, Top. Catal. 15 (2001) 103.
[16] H. Roussel, B. Mehlomakulu, F. Belhadj, E. van Steen, J.M.M. Miller, J. Catal. 205 (2002) 97.
[17] M.O. Guerrero-Pérez, J.L.G. Fierro, M.A. Vicente, M.A. Bañares, J. Catal. 206 (2002) 339.
[18] S. Hansen, K. Ståhl, R. Nilsson, A. Andersson, J. Solid State Chem. 102 (1993) 340.
[19] A.R. Landa-Canovas, J. Nilsson, S. Hansen, K. Ståhl, A. Andersson, J. Solid State Chem. 116 (1995) 377.
[20] L. Vegard, Phil. Mag. Ser. 6 (32) (1916) 65.
[21] W.H. Baur, Cryst. Rev. 13 (2007).
[22] B.G. Hyde, S. Andersson, Inorganic Crystal Structures, Wiley, New York, 1989.
[23] H. Schüer, W. Klemm, Z. Anorg. Allg. Chem. 395 (1973) 287.
[24] T. Birchall, A.W. Sleight, Inorg. Chem. 15 (1976) 868.
[25] F.J. Berry, M.E. Brett, Inorg. Chim. Acta 76 (1983) L205.
[26] J. Nilsson, A.R. Landa-Cánovas, S. Hansen, A. Andersson, Catal. Today 33 (1997) 97–108.
[27] A.R. Landa-Canovas, S. Hansen, K. Ståhl, Acta Crystallogr. B53 (1997) 221–230.
[28] F.J. García-García, A.R. Landa-Cánovas, S. Hansen, L.C. Otero-Díaz, submitted for publication.
[29] A.V. Hariharan, D.R. Powell, R.A. Jacobson, H.F. Franzen, J. Solid State Chem. 36 (1981) 148.
[30] M.O. Guerrero-Pérez, M.A. Bañares, J. Phys. Chem. C 111 (2007) 1315.
[31] M.O. Guerrero-Pérez, M.A. Bañares, Catal. Today 96 (2004) 265.
[32] M.O. Guerrero-Pérez, M.A. Bañares, Chem. Commun. (2002) 1292.